International Journal of Technology 14(1) 26-37 (2023)
Received October 2019 / Revised May 2022 / Accepted July 2022

International Journal of Technology

The Effects of Effective Thermal Conductivity of Porous Materials Under Vapor Flow in Sudden Enlargement-Contraction Channel on Local Heat Transfer

Eko Siswanto[1*], Denny Widhiyanuriyawan[1], Mochammad Agus Choiron[1], Djarot Bangun Darmadi[1], Yasuo Katoh[2]

[1]*Mechanical Engineering Departmen,t Faculty of Engineering, Brawijaya University, Jalan MT. Haryono No. 167, Malang 65145, Indonesia*
[2]*Mechanical Engineering Department, System Design and Engineering, Yamaguchi University, Tokiwadai 2-16-1, Yamaguchi 7558611, Japan*

Abstract. This study aims to obtain the local heat penetration and local heat convection characteristics in a system where a flow of heated vapour cedes thermal energy to a horizontal heat-sink plate. The heat penetrates a bed of porous materials with variations in the thermal conductivity inside a sudden-enlargement-contraction-channel. The two non-dimensional parameters of interest are the local Nusselt and Metais-Eckert numbers. The solid particles used for the porous bed are copper, carbon steel, and ceramics. The study is conducted numerically via the software package Ansys-Fluent to solve the Navier-Stokes equation for the conservation of mass, momentum, and energy to obtain the profiles of local temperature and velocity, both in the porous bed and in the vapour stream. Results of this study show that the overall effective-thermal-conductivity of porous materials filled with vapour mainly affects the local Nusselt number. The local Nusselt number increases with increasing overall effective thermal conductivity of porous materials. The sudden enlargement-contraction of the channel affects the local Metais-Eckert number. This finding is proven by the average Metais-Eckert number's variation along the duct and by its non-proportionality to the overall-effective-thermal-conductivity of each porous material. Together with the local Reynolds number, the local Metais-Eckert number describes the flow regimes that locally occur in the system, namely, transitional-combined-convection, laminar-combined-convection, and laminar-forced-convection. Additionally, based on the local Nusselts number, this study locates the critical point of change from enlargement-affected-zone to contraction-affected-zone at 80 mm along the duct's axis, which means that the switchover-point is not at the centre of the channel.

Keywords: Effective thermal conductivity; Metais-Eckert number; Porous materials bed; Sudden enlargement-contraction channel

1. Introduction

Because of their importance in industrial applications, research and development projects on porous materials are carried out. Among the most notable research works in the literature is the paper by Zulkarnain, Sharudin, and Ohshima (2022). They show that polymer foams have superior properties in low density by using, as basic material,

*Corresponding author's email: eko_s112@ub.ac.id, Tel.: +62 341 587710, 587711; Fax: +62 341 551430
doi: 10.14716/ijtech.v14i1.3660

thermoplastic elastomer Polystyrene-b-polybutadiene-b-polystyrene (SEBS) foams. Successively, Zulkarnain, Fadzil, and Sharudin (2017) have developed a pores distribution model for the thermal conductivity analysis and measurement of polypropylene porous materials. In addition, Muharam *et al.* (2018) researched porous adsorbents used for natural gas adsorption in gas storage technologies.

In line with the development of science and technology on heat transfer, the usage of porous or permeable materials has replaced the extended solid slab method (Kundu *et al.*, 2012; Bassam and Hijleh, 2003; Kiwan and Al-Nimr, 2001). The idea behind the slab method of increasing the heat transfer by expanding the surface area available to the heat transfer through solid slabs finds its limitation in space availability. In contrast, a porous material provides a much bigger surface area for heat transfer.

A good knowledge of a system's local heat transfer characteristics is required to create a more accurate design and better control of heat release from a heat source to a heat sink. This is the case, for example, in heat exchangers at the inlet and outlet sections or in a heat releaser's regions where sudden changes in shape occur. In a porous media system, heat penetration and heat convection play a dominant role in heat transport (Siswanto, Katsurayama, and Katoh, 2011a). Therefore, the present study focuses on determining the characteristics of local heat penetration and local heat convection in a system where a heated vapour moves inside a sudden-enlargement-contraction-channel and transfers its thermal energy to a horizontal heat-sink plate penetrating a bed of porous materials. The study also accounts for variations in the porous material's thermal conductivity.

Porous materials have porous and capillary holes scattered throughout a solid volume, resulting in cavities where flows of mass and energy can occur. Slabs made from porous materials have a higher ratio of surface area to volume than those built out of a continuum solid. Several experimental and numerical studies on fluids used as heat sources flowing tangentially over porous material bed layers exist in the literature. Among the experimental studies are worth mentioning those by Nagata *et al.* (2013), Siswanto, Katsurayama, and Katoh (2011b), Siswanto, Katsurayama, and Katoh (2010) where the heat transfer on laminar condensation using a bed of porous materials was indagated. More specifically, in the experiments carried out, the authors did flow a saturated vapour stream over glass beads and alumina balls with different thermal conductivity and wettability to obtain the characteristic curves of condensate-propagation and heat-flow that penetrates the porous materials bed in a channel. Results allowed the authors to understand how the propagation characteristics of the condensate flow are affected by the materials' wettability. Propagation can be linear dominant, nonlinear dominant, or chaotic. However, this level of information about the heat flow characteristics in the system is still inadequate. The heat flow characterization made in terms of its Jacob or Kutaleladze numbers or via some perturbation parameters like those determined by Kaviany (Siswanto, Katsurayama, and Katoh, 2011a) is still based on some non-dimensional numbers generally defined by differences between the average temperature values along the channel.

The studies mentioned above on heat transfer with saturated vapour (Siswanto *et al.*, 2016; Nagata *et al.*, 2013; Siswanto, Katsurayama, and Katoh, 2011a; Siswanto, Katsurayama, and Katoh, 2010) report Jacob number values of less than 100. This finding means that, although the propagation of condensate into the porous media is affected by the wettability of materials, the condensation from saturated vapour to liquid is predominantly controlled by heat transfer rather than by viscous inertia (Siswanto, Katsurayama, and Katoh, 2011a). Those studies though, do not present the effect and contribution of the effective-thermal-conductivity on the local heat transfer. Hence, this study focuses on the effect of the materials' effective-thermal-conductivities (instead of

wettability) on the local heat transfer in a channel where a stream of saturated vapour flows over a bed made from various porous materials

Yamaguchi, Katoh, and Kurima (2007) and Katoh *et al.* (2007) measured the effective thermal conductivity of porous materials in the presence of two different thermodynamic states of the fluid flowing through the voids inside two thicknesses of a layer of porous material. Based on Yamaguchi's work, the measurements of effective-thermal-conductivity of porous material in this study are correlated as in equations (1), (2), and (3):

$$\frac{k'_{ef}}{k_p} = (1-\varepsilon^{2/3}) + \frac{\varepsilon^{2/3}}{\left\{(1-\varepsilon^{1/3}) + \varepsilon^{1/3}\left(\frac{k_p}{k_{v1}}\right)\right\}} \tag{1}$$

$$\frac{k''_{ef}}{k_p} = (1-\varepsilon^{2/3}) + \frac{\varepsilon^{2/3}}{\left\{(1-\varepsilon^{1/3}) + \varepsilon^{1/3}\left(\frac{k_p}{k_{v2}}\right)\right\}} \tag{2}$$

$$\overline{k_{ef}} = \frac{k'_{ef}\, k''_{ef}}{k'_{ef}\left(\frac{\bar{\delta}}{z}\right) + k''_{ef}\left\{1-\left(\frac{\bar{\delta}}{z}\right)\right\}} \tag{3}$$

The term k'_{ef} in expression (1) is the effective thermal conductivity of the average thickness of the bed upper layer $\left(z - \bar{\delta}\right)$ penetrated by the hotter vapour. Due to gravity and its higher temperature, the vapour at thermodynamic state 1 has a smaller density ρ_{v1} and smaller specific weight γ_{v1}. The term k''_{ef} in expression (2 is the effective thermal conductivity of the average-thickness of the bed lower layer $\bar{\delta}$ through which the cooler vapour in the thermodynamic state 2, with larger specific weight γ_{v2} and density ρ_{v2}, and thermal conductivity k_{v2} flows. Furthermore, $\overline{k_{ef}}$ in (3) is the overall effective thermal conductivity of the total bed thickness z, penetrated by the vapour flow in the two thermodynamic conditions mentioned above.

To better explore the influence of the bed material thermal conductivity on results, we have selected for the present study three materials which cover a broad spectrum of thermal conductivity values, namely copper with k_{Cu}=385 (W/mK), carbon steel with k_{cs}=43 (W/mK), and ceramics with k_{cer}=1.298 (W/mK). The selected materials represent high, medium, and low thermal conductivities, respectively. The choice of these materials is made to obtain clear information on the effect of thermal conductivity and does not involve changes in wettability, as in already cited previous studies, which made use of materials with only slightly different values of thermal conductivity, (i.e., glass beads with k_{gb}=1.035 (W/mK) and alumina balls with k_{ab}=18.84 (W/mK)).

To obtain details on the local heat transfer characteristics along the channel, for the porous bed upper surface and the inside (i.e., void) of the porous material bed the overall effective thermal conductivity k_ef is used. In the present study, the Navier-Stokes system of equations for the conservation of mass, momentum, and energy in the saturated vapour flow is solved. With this approach, an ideally infinite number of observation points can be obtained, with detailed information such as local temperatures, local pressures, local velocities, and some local properties of the saturated vapour for a variety of pressure and temperature values.

2. Methods

2.1. Materials, Procedures, and Test section

This investigation uses three different porous beds made of copper (Cu), carbon steel (cs), and ceramics (cer) particles with thermal conductivity k_{Cu} = 385 (W/mK), k_{cs} = 43

(W/mK) and k_{cer} = 1.298 (W/mK), respectively. The thermal conductivity of the saturated vapour k_v is assumed to be 0.0206 (W/mK). The particles constituting the porous beds are spherical, with a diameter ϕ of 10^{-3} (m). The porosity ε of each bed is assumed to be constant and fixed at 0.38. The saturated vapour streams over the upper surface of the porous bed from the inlet section with temperature T_{in}= 323 (K), whereas the temperature of the copper plate at the bottom of the bed T_b is kept at 283 (K).

The temperature T_∞ of the ambient surrounding the simulated chamber is fixed at 293 (K). Viscous no-slip wall boundary conditions are imposed on the chamber's upper, front, and back walls. The chamber has dimensions 240x10^{-3} (m) in length L, 20x10^{-3} (m) in width W, and 40x10^{-3} (m) in height H. The size of the porous bed that occupies the chamber's volume is 240x10^{-3} (m) in length l, 20x10^{-3} (m) in width w, and 20x10^{-3} (m) in height z. The saturated vapour enters the chamber with an inlet velocity U_{in} 2.5 (m/s) and a pressure P_{in} of 1 (atm) through a hole of diameter d_i= 8x10^{-3} (m). The vapour exits the chamber through a hole of diameter d_o= 8x10^{-3} (m).

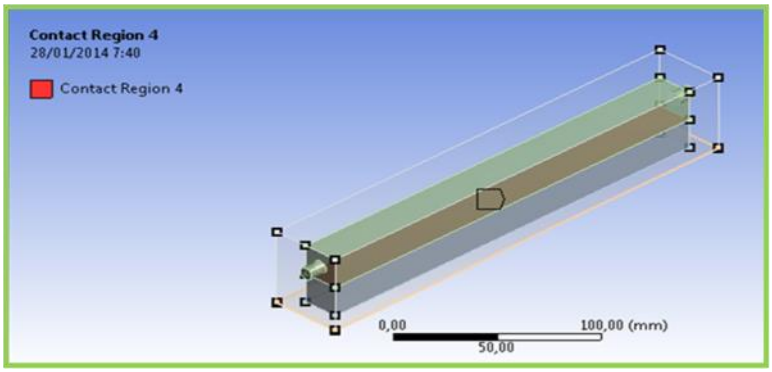

Figure 1 Test section

As previously stated, the saturated vapour flow is subjected to a sudden expansion as it enters the chamber. di_H represents the chamber's inlet hydraulic diameter, and D_H is the hydraulic diameter of the duct channel through which the vapour flows. One can then compute the enlargement ratio of the duct to the inlet's hydraulic diameter D_H/di_H whose value is 2.5. At the channel outlet, the saturated vapour goes through a sudden contraction. The contraction ratio of the outlet's hydraulic diameter do_H to the duct's hydraulic diameter (do_H/D_H) is 0.4.

Figure 1 depicts the installation of the porous bed, the channel of saturated vapour, and the chamber of the test section. The same figure shows the glass-made test section walls (with a thickness t_h of 10x10^{-3} (m)) in transparent colour. The light green colour refers to the duct channels of saturated vapour, while the grey colour indicates the porous bed. The dark green colour is the contact region between the vapour stream and the porous bed's upper surface. The copper plate is in contact with the porous bed's bottom face (not visible in the figure). Finally, Figure 2 reports the flowchart of the model of this current study.

2.2. Computation, Governing Equations, and Flowchart of Model

The software ANSYS Workbench 18.1 (Academic Research license) is used to compute the local temperature gradient, local property parameters, and heat transfer both in the porous materials bed and the saturated vapour stream. Brick-type 8-node-elements are used for meshing the porous materials bed, the volume occupied by the saturated vapour, the chamber walls, and the bottom of the copper plate (ANSYS Inc., 2017). The CONTA174 (ANSYS Inc., 2017) allows us to define the contact and sliding regions between the saturated vapour stream and the porous bed upper surface, between walls and vapour, between walls and porous material bed, and between the porous bed and copper plate. This method allows

for an analysis of the coupled field at the contact region. Figure 1 also shows the contact region between the vapour and the upper surface of the porous bed.

This ANSYS solves the Navier-Stokes conservation equation for mass, momentum, and energy in the saturated vapour flow with heat transfer. The following paragraphs give a brief review of those equations.

Under the hypothesis that no other mass is added to the system, the mass conservation equation for the compressible saturated vapour writes (ANSYS Inc., 2017; Welty *et al.*, 2008),

$$\frac{\partial \rho}{\partial t} + \nabla.(\rho \vec{v}) = 0 \tag{4}$$

ρ is the vapour density, t is the time, and $\vec{v}$ is the velocity field. Under the assumption that no forces act on the vapour other than inertial and viscous forces, the momentum conservation equation in an inertial reference frame writes (ANSYS Inc., 2017; Welty et al, 2008),

$$\frac{\partial}{\partial t}(\rho \vec{v}) + \nabla.(\rho \vec{v}\vec{v}) = -\nabla P + \nabla.(\bar{\bar{\tau}}) \tag{5}$$

P is the static pressure and $\bar{\bar{\tau}}$ is the stress tensor that can be written as,

$$\bar{\bar{\tau}} = \mu\left[(\nabla \vec{v} + \nabla \vec{v}^T) - \frac{2}{3}\nabla.\vec{v}I\right] \tag{6}$$

μ is the vapour molecular (dynamic) viscosity, the term of the $(\nabla \vec{v}^T)$ refers to the volume dilation effect, and I is the unit tensor.

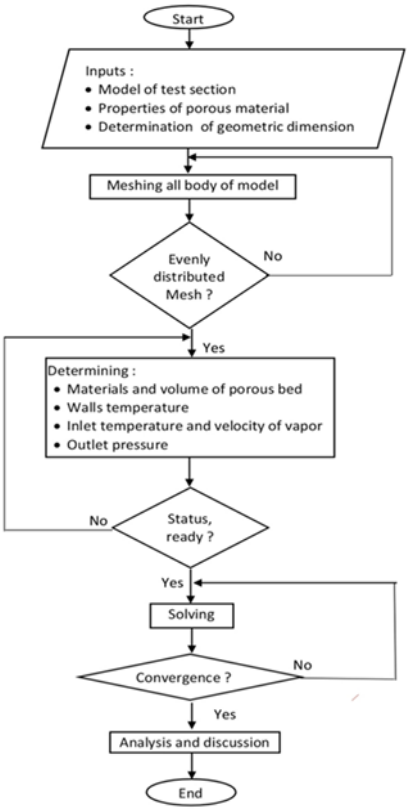

Figure 2 Flowchart of model

Under the assumption that no heat source exists in the test section other than the heated saturated vapour, the energy conservation equation in terms of sensible enthalpy ξ writes (ANSYS Inc., 2017),

$$\frac{\partial}{\partial t}(\rho\xi) + \nabla.(\rho\xi\vec{v}) = \nabla.[(k_{v_l} + k_{v_t})\nabla T] \tag{7}$$

where k_{v_l} and k_{v_t} are the saturated vapour molecular (laminar) and turbulent thermal conductivities.

Finally, Figure 2 shows the model's flowchart for the current study.

3. Results and Discussion

3.1. Local Nusselts Numbers

The local Nusselt number Nu_x writes:

$$Nu_x = \frac{Q_{cx}\ D_{Hx}}{k_{vx}\ (T_x - T_{wx})} \tag{8}$$

Where Q_{cx} is local heat convection, D_{Hx}, k_{vx}, T_x, and T_{wx} are the channel's local hydraulic diameter, the vapour's local thermal conductivity and temperature, and the local temperature of the porous bed's upper surface. With reference to the convection map based on Metais-Eckert's work (Holman, 2010), the physical behaviour of the saturated vapour is divided into two types, namely transitional and laminar flow. Therefore, formulas used in the present work for computing the local Nusselt numbers Nu_x are those valid for transitional and laminar flows.

For the transitional flow, local Nusselt numbers $Nu_x$are evaluated by calculating the average Nusselt numbers $\overline{Nu_E}$ according to the empirical formula given in Engineering Science Data Unit (ESDU) and from Hallquist's experiment (Hallquist and Meyer, 2011). The local Nusselt number in the laminar flow regime is calculated from the average local Nusselt numbers $\overline{Nu_P}$ as in Petukhov's and Hallquist's experiments (Hallquist and Meyer, 2011).

The average Nusselts number $\overline{Nu_E}$ in transitional flow, from ESDU and Hallquist and Meyer's (2011)'s experiment, writes,

$$\overline{Nu_E} = \Psi\, Nu_{Lx} + (1 - \Psi) Nu_{Tx} \tag{9}$$

Ψ, Nu_{Lx}, and Nu_{Tx} are obtained by:

$$\Psi = 1.33 + \left(\frac{Re_x}{6000}\right) \tag{10}$$

The Nu_{Lx} is local Nusselt number in laminar combined convection (Hallquist and Meyer, 2011) that, according to Oliver's experiment in Holman (2010), can be written as:

$$Nu_{Lx} = 1.75\left(\frac{\mu_{fx}}{\mu_{wx}}\right)^{0.14}\left[[Gz_x + 0.0083\,(Gr_x Pr_x)^{0.75}]\right]^{1/3} \tag{11}$$

Where μ_{fx} and μ_{wx} are the vapours' local dynamic viscosity at local film temperature, $T_{fx} = (T_x + T_{wx})/2$, and at the porous bed's upper surface temperature T_{wx}. The local Graetz number Gz_x is given as:

$$Gz_x = Re_x\, Pr_x\, \frac{D_{Hx}}{L_x} \tag{12}$$

Nu_{Tx} is the local Nusselt number in the turbulent combined convection regime as suggested by Hallquist and Meyer (2011) based on Metais and Eckert's experiment (Holman, 2010), that can be defined as follows:

$$Nu_{Tx} = 4.69\, Re_x^{0.27} Pr_x^{0.21} Gr_x^{0.07} \left(\frac{D_{Hx}}{L_x}\right)^{0.36} \quad (13)$$

Finally, the average local Nusselts number $\overline{Nu_P}$ in a laminar flow proposed in Petukhov's experiment (Hallquist and Meyer, 2011) can be written as

$$\overline{Nu_P} = 4.36 \left[1 + \left(\frac{Ra_x}{1800}\right)^4\right]^{0.045} \quad (14)$$

here, Ra_x is the local Rayleigh numbers, defined as:

$$Ra_x = Gr_x\, Pr_x \quad (15)$$

Figure 3 shows the computed local $\overline{Nu_E}$ and $\overline{Nu_P}$ numbers versus the average ESDU's empirical formula and Petukhov's experiment of $Nu(x)_E$ = 6.29 and $\overline{Nu(x)_P}$ = 4.5, respectively. Figure 3 shows that the local Nusselt number Nu_x closer to the reference line is for the porous carbon steel case ($\overline{Nu_{x_{cs}}}$), whose overall average value is 3.32. The overall local Nusselt number average value in the porous-copper case ($Nu_{x_{cu}}$= 46.08) is higher than the reference, while in the case of the porous ceramic, the computed value is under both lines with $\overline{Nu_{x_{cer}}}$= 0.07. There is a reason for these findings. Formulas given by ESDU $\overline{Nu_E}$ or Petukhov $\overline{Nu_P}$ derive from a horizontal straight pipe made of solid carbon steel, so it makes sense that their predicted values are close to the overall average of the porous-carbon-steel's $\overline{Nu_{x_{cs}}}$. In addition, even though Petukhov's experiment uses a straight horizontal pipe and this study a horizontal channel with a sudden change of area, the pipe's and channel's materials are the same. It is no surprise that results in terms of the overall average of Petukhov's Nusselt numbers ($\overline{Nu(x)_P}$ = 4.5) are close to those obtained with porous-carbon-steel ($\overline{Nu_{x_{cs}}}$ = 3.32) so that one can use those empirical formulas for the validation of the simulation results in the present study. The same consideration is not valid in the copper (48.06) and ceramic (0.07) cases, as the porous materials used in the experiments and the simulation are different.

Regarding the values of $\overline{Nu_{x_{cer}}}$, $\overline{Nu_{x_{cs}}}$, and $\overline{Nu_{x_{Cu}}}$, it can be seen that Nu_xincreases with increasing overall-effective-thermal-conductivity $\overline{k_{ef}}$ of porous materials. This finding is also understandable because, due to the local convection, heat Q_{cx} in the vapour can transfer easier and faster through a porous material with higher $\overline{k_{ef}}$. In other terms, a high overall effective thermal conductivity represents the porous material's heat-penetrability.

Furthermore, one can drive an important piece of information from the local Nusselt numbers $\overline{Nu_{x_{cs}}}$ in the porous carbon steel case. One wants to determine the position of a neutral point, a point free from the influence of the channel's sudden enlargement and sudden contraction. Moreover, one can assume that the point's position coincides with the prediction of ESDU $\overline{Nu_E}$ or the Petukhov $\overline{Nu_P}$ since $\overline{Nu_E}$ and $\overline{Nu_P}$ are based on a horizontal straight pipe made of carbon steel. An exam of the computed results shows that the neutral point is situated at x ≈ 80 (mm) along the channel. The neutral point can also be regarded as a switchover point from the influences of the channel's sudden enlargement and sudden contraction. The location of the neutral point at x ≈ 80 (mm) also shows that the point is not at the channel's midspan.

We can further validate the simulation results by comparing the average local Nusselt numbers Nu_x of the present study with the average Nusselt numbers measured in a previous experiment in a sudden enlargement contraction channel by Siswanto, Katsurayama, and Katoh, (2011a). One can make the comparison because the vapour's temperature during the previous experiment and in the simulated cases is the same (323 (K)). Moreover, the thermal conductivity value of the porous ceramics bed used in this

study compares well with that of the porous glass beads bed of the previous experiment (k_{cer} = 1.298 (W/mK), k_{gb} = 1.035 (W/mK)). Both Nusselt number averages follow equation (8), but the T_x and T_{wx} values that compare in the equation are substituted with the vapour's average temperature and the average temperature of the porous bed's upper surface along the channel. Figure 3 shows that the curve of the average local Nusselt number computed in this study is very close to the curve obtained from the previous experiment. This finding further validates the results of the current study.

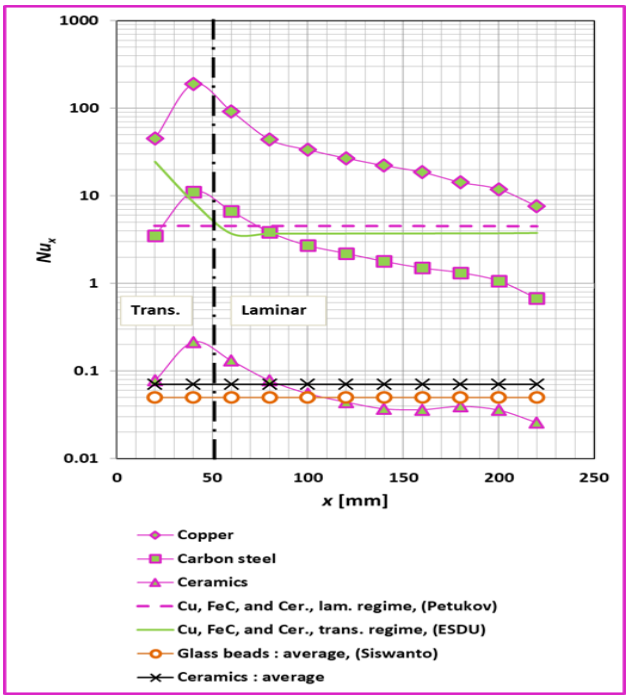

Figure 3 The local Nusselt number Nu_x in transitional and laminar flow regimes compared with Nusselt numbers from Petukhov's experiment $\overline{Nu_P}$ and from ESDU's empirical formula $\overline{Nu_E}$ using a carbon steel straight pipe. Average of Nusselt numbers from the current study using porous ceramics bed compared with Siswanto's experiment in a sudden enlargement-contraction channel using porous glass beads bed

3.2. Metais-Eckert Numbers

An experiment from Metais and Eckert provides the value of the Metais-Eckert numbers (ME) by measuring the magnitude of the vapour's convection heat rate against the length of the channel. The study also correlates the local Metais-Eckert number values ME_x with the channel's shape, as the channel enlarges suddenly after the inlet and shrinks abruptly before its outlet. The correlation formula, as defined by Metais and Eckert (Holman, 2010) is:

$$ME_x = Gr_x\, Pr_x\, \frac{D_{Hx}}{L_x} \tag{16}$$

The ME_x characteristics for the three porous materials along the channels are shown in Figure 4, where a strong variation of the ME_x values along the channel is visible. To simplify the discussion on the ME_x variation, the channel length is divided into two half areas A and B also represented in Figure 4.

Analysis of Figure 4 shows that inside area A the porous material with the highest $\overline{ME_x}_A$ number is copper ($\overline{ME_x}_{Cu,A}$ = 19,360.12 > $\overline{ME_x}_{cs,A}$ = 18,911.19 > $\overline{ME_x}_{cer,A}$ = 18,795.16). This is different from what is found in the second half of the channel length, where in order of magnitude the average of Metais-Eckert numbers along the B area $\overline{ME_x}_B$ is $\overline{ME_x}_{Cu,B}$ = 18,957.54 > $\overline{ME_x}_{cer,B}$ = 17,653.71 > $\overline{ME_x}_{cs,B}$ = 12,324.95. The different order in

the ME_x distribution along the areas A and B, and the corresponding variations in the amplitudes of the curves of ME_x suggest that, in the convective heat transfer over the porous materials, the role of the porous materials' overall effective thermal conductivity $\overline{k_{ef}}$ is negligible. This statement is proven by the fact that the ME_x values and each of the porous materials' overall effective thermal-conductivity $\overline{k_{ef}}$ are not in the same order. Therefore, a further analysis based on the ME_x value variation with convective parameters is required.

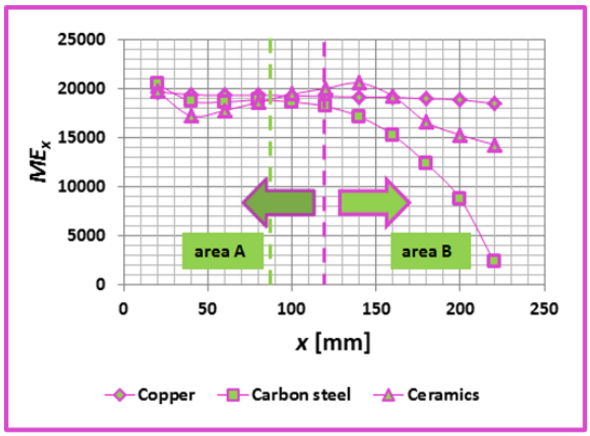

Figure 4 Local Metais-Eckert numbers ME_x throughout the bed made of porous materials

With reference to equation (16) and under the assumption that D_{Hx} and L_x are constant, and that the local Prandtl number Pr_x does not change significantly along the channel, then the cause of variation of the ME_x in the A and B areas is the variation of local Grasshoff numbers Gr_x. The definition of Gr_x is:

$$Gr_x = \frac{g_x \beta_x (T_x - T_{wx}) D_{Hx}^3}{\nu_x^2} \tag{17}$$

Therefore, by assuming constant the gravity acceleration g_x and hydraulic diameter D_{Hx}, and considering the changes of the local volume expansivity β_x with the temperature, one can conclude that the variation of ME_x is affected by the temperature difference of $(T_x - T_{wx})$ and the square of the local kinematic viscosity ν_x. Equation (17) shows that the effect on the ME_x variation due to the temperature difference $(T_x - T_{wx})$ is linear, whereas the dependence on kinematic viscosity $\overline{\nu_x}^2$ is squared. The present study finds that the contribution of average changes of the local kinematic viscosity $(\overline{\nu_x}^2)$ to the average Grasshoff number $\overline{Gr_x}$ can be up to 8,234.35 times that due to the temperature difference $(T_x - T_{wx})$ for all the examined porous materials. Therefore, one can conclude that the dynamic changes in the value ME_x in the A and B areas are predominantly due to changes in local kinematic viscosity ν_x of the saturated vapour.

3.3. Convection and Flow Regimes

In this part of the study, mapping of the convective flow regimes based on the value of local Metais-Eckert numbers ME_x, i.e., based on Metais' and Eckert's experiment (1964), and local Reynolds numbers Re_x, have been conducted, as shown in Figure 4. Re_x is defined as follows:

$$Re_x = \frac{U_x D_{Hx}}{\nu_x} \tag{18}$$

Local convection exists along the first 40 (mm) in the channel, i.e., evaluated at x=20 (mm) and x=40 (mm). For all types of porous materials, the local Reynolds number range is 873.97 ≤ Re_x ≤ 2,222.74, and the local Metais-Eckert number range is 17,232.48 ≤ ME_x ≤ 20,451.59. As for Metais's and Eckert's experiment (Holman, 2010), if ME_x is between ~15,000 and ~50,000 and Re_x is between ~700 and ~4,000, then all the local convective phenomena belong either to the combined-convection or the transitional-flow regimes. As a side note, if the combined convection falls in this ME_x range, then a transitional flow regime can be observed to occur below 2,000 (Holman, 2010). This situation is represented in quadrant-I of the map in Figure 5.

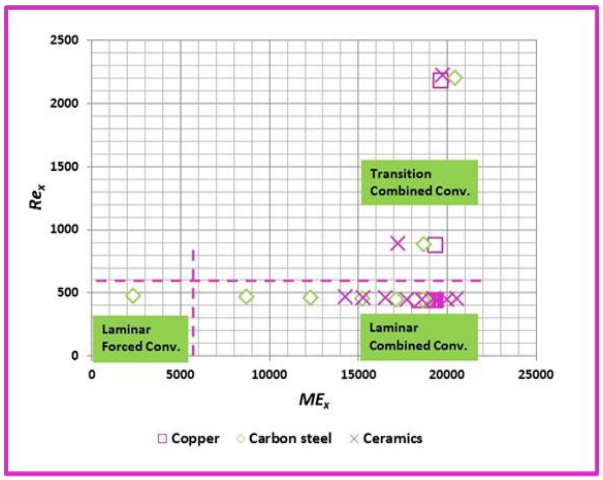

Figure 5 Mapping of laminar forced convection, laminar combined convection, and transition combined convection regimes based on Metais and Eckert

Moving deeper inside the channel and at the axial coordinate 60 (mm) ≤ x ≤ 200 (mm) ranges of local Reynolds and Metais-Eckert numbers are 437.22 ≤ Re_x ≤ 464.78 and 8,715.32 ≤ ME_x ≤ 19,305.57 respectively. As per the references (Holman, 2010), if ME_xexceeds ~4,000 in the region of Re_xsmaller than ~600, the convection regime becomes combined-convection in a laminar-flow-regime. This situation lies in quadrant IV on the map.

Furthermore, a non-uniform local convection regime occurs in the channel at x = 220 (mm). At this point, the values of (ME_x ; Re_x) for porous copper and ceramic materials are (18,458.33; 440.04) and (14,288.95; 465.61), respectively. This finding puts the local convection for porous-copper and porous ceramics materials in the combined convection regime with laminar flow due to ME_x exceeding ~4,000 and Rex being smaller than ~600. This point also lies on quadrant-IV of the map. This combined convection regime, however, does not occur in the case of convection above porous carbon steel. The value of (ME_x ; Re_x) for porous-carbon-steel is (2,343.63; 476.61). It means that the value of ME_x is less than ~4,000, and the Re_x is smaller than ~600. Referring to Metais and Eckert in Holman (2010) this condition can be categorized as forced convection in laminar flow, and it is the only case that lies on quadrant-III of the map.

Finally, we can summarize the results of the present study. Table 1 presents a recapitulation of what has been found in the course of the study.

Table 1 Recapitulation of results obtained in the present study

Name	Materials of Porous Bed		
	Copper	Carbon Steel	Ceramics
Overall-average of Nusselts numbers	$\overline{Nu_{x_{Cu}}}$= 46.08	$\overline{Nu_{x_{cs}}}$= 3.32	$\overline{Nu_{x_{cer}}}$ = 0.07
Average of Metais-Eckert numbers along the A area	$\overline{ME_{x_{Cu,A}}}$ = 19,360.12	$\overline{ME_{x_{cs,A}}}$ = 18,911.1	$\overline{ME_{x_{cer,A}}}$= 18,795.16
Average of Metais-Eckert numbers along the B area	$\overline{ME_{x_{Cu,B}}}$ = 18,957.54	$\overline{ME_{x_{cs,B}}}$ = 12,324.95	$\overline{ME_{x_{cer,B}}}$ = 17,653.71
Convection and flow regimes [ME_x ; Re_x] along $x \leq 40$ (mm)	[(17,232.48 ≤ ME_x ≤ 20,451.59); (873.97 ≤ Re_x ≤ 2,222.74)]	[(17,232.48 ≤ ME_x ≤ 20,451.59); (873.97 ≤ Re_x ≤ 2,222.74)]	[(17,232.48 ≤ ME_x ≤ 20,451.59); (873.97 ≤ Re_x ≤ 2,222.74)]
Convection and flow regimes [ME_x ; Re_x] along 60 (mm) ≤ x ≤ 200 (mm)	[(8,715.32 ≤ ME_x ≤ 19,305.57); (437.22 ≤ Re_x ≤ 64.78)]	[(8,715.32 ≤ ME_x ≤ 19,305.57); (437.22 ≤ Re_x ≤ 464.78)]	[(8,715.32 ≤ ME_x ≤ 19,305.57); (437.22 ≤ Re_x ≤ 464.78)]
Convection and flow regimes [ME_x ; Re_x] in x=220 (mm)	[(18,458.33); (440.04)]	[(2,343.63); (476.61)]	[(14,288.95); (465.61)]

4. Conclusions

Previous results and discussion allow us to establish relations between the effective thermal conductivity of porous materials under saturated vapour in a sudden enlargement-contraction channel with the local Nusselts numbers, the local Metais-Eckert numbers, and the local convection flows regimes. The local Nusselt numbers Nu_x in the channel are affected by the porous material overall-effective-thermal-conductivity $\overline{k_{ef}}$, where the term $\overline{k_{ef}}$ can also represent the heat penetrability of the porous materials. Variations of the local Metais-Eckert numbers ME_x are mostly influenced by the local vapour kinematic viscosity ν_x, where ν_x is affected by the shape of the sudden-changed-channel. Although the inlet velocity and temperature are constant, the co-effect of the overall effective thermal conductivity and the abrupt change of the channel shape results in local variations of the Reynolds and Metais-Eckert numbers. Their combinations, in turn, translate into different physical regimes for both the type of fluid flow and the type of convection heat transfer, namely, transitional combined-convection, laminar combined-convection, and laminar forced convection. Finally, as an additional important piece of information, based on the average of local Nusselt numbers of porous carbon steel $\overline{Nu_{x_{cs}}}$, ESDU's $\overline{Nu_E}$, and Petukhov's $\overline{Nu_P}$, we can obtain the location of the Nu_x critical point for the porous carbon steel. This point is the location of change from an enlargement-affected zone to a contraction-affected one. Its position is at $x \approx 80$ (mm), (area A), not in the middle of the channel.

Acknowledgments

The authors are obliged to thank the Brawijaya University, Malang, Indonesia, for providing the laboratory facilities, ANSYS Academic Research license software and the Ministry of Research, Technology, and Higher Education, Indonesia, via the Engineering Faculty of Brawijaya University, for the financial support to the present research under the grant number 134/UN10.F07/PN/2018.

The authors would also like to thank all the members of the porous media team, with particular mention to Rizki Ferdiantara, for their fundamental role in providing data.

References

ANSYS Inc., 2017. *CFX 18.1 user's guide*. Canonsburg, Pennsylvania, USA: ANSYS

Bassam, A., Hijleh, KA., 2003. Natural convection heat transfer from cylinder with high conductivity permeable fin. *Journal of Heat Transfer,* Volume 125 (2), pp. 282–288

Hallquist, M, Meyer, J.P., 2011. *Heat transfer and pressure drop characteristics of smooth tubes at a constant heat flux in the transitional flow regime.* Master Thesis, University of Pretoria, South Africa

Holman, J.P., 2010. *Heat transfer*. 10th edition. Mc. Graw-Hill

Katoh, Y., Kurima, J., Yamaguchi, S., 2007. Study on the condensation phenomena on a horizontal cooled flat plate in porous medium (in Japanese). *In*: Proceeding of 44th National Heat Transfer Symposium, Japan, 3, pp. 571–572

Kiwan, S., Al-Nimr, M.A., 2001. Using porous fin for heat transfer enhancement. *Journal of Heat Transfer*, Volume 123(4), pp. 790–795

Kundu, B., Bhanja, D., Lee, KS., 2012. A model on the basis of analytics for computing maximum heat transfer in porous fins. *International Journal of Heat and Mass Transfer*, Volume 55, pp. 7611–7622

Muharam, Y., Kusrini, E., Saubryani, N., Ulfa, M., 2018. Simulation of a metal organic framework-based adsorbed natural gas storage tank. *International Journal of Technology*, Volume 9(2), pp. 412–421

Nagata, R., Siswanto, E., Katsurayama, H., Katoh, Y., 2013. Study on condensation of mixed vapor on flat cooling plate in porous media -Influence on surface texture (Wettability) of porous media. *In*: Proceding The 24th International symposium on Transport Phenomena, Japan

Siswanto, E., Angga, V.R., Choiron, M.A., Nagata, R., Katsurayama, H., Katoh, Y., 2016. Convective regimes on porous media within sudden changed channel due to tangential gas flow. *Applied Mechanics and Materials*, Volume 836, pp. 96–101

Siswanto, E., Katsurayama, H., Katoh, Y., 2010. Forced laminar convective condensation in porous media. *In*: Proceding 47th National Heat Transfer Symp., Japan, 47, pp. 135–136

Siswanto, E., Katsurayama, H., Katoh, Y., 2011(a). Instability on condensate propagation in porous media. *International Journal of Mechanics*, Volume 4(5), pp. 327–335

Siswanto, E., Katsurayama, H., Katoh, Y., 2011(b). Laminar condensation in porous media with ambient treatments. *JP Journal of Heat and Mass Transfer*, Volume 5(2), pp. 149–168

Welty, J.R., Wicks, C.E., Wilson, R.E., Rorer, G.L., 2008. *Fundamentals of momentum, heat and mass transfer,* 5th edition. John Wiley and Sons

Yamaguchi, S., Katoh, Y., Kurima, J., 2007. *Study on heat and mass transfer in porous media on a horizontal plate (in Japaneese).* Master's Thesis, Yamaguchi University, Japan.

Zulkarnain, M., Fadzil, M.A., Sharudin, R., 2017. Algorithm of pores distribution model for analysis and measurement of thermal conductivity of polypropylene porous material. *International Journal of Technology,* Volume 8(3), pp. 398–407

Zulkarnain, M., Sharudin, R.W., Ohshima, M., 2022. Towards understanding of pore properties of polystyrene-b-polybutadiene-b-polystyrene (SEBS) foam effect on thermal conductivity using numerical analysis. *International Journal of Technology,* Volume (13)3, pp. 533–543